Chemistry–A European Journal
Research Article
doi.org/10.1002/chem.202200687
Chemistry Europe
European Chemical Societies Publishing
www.chemeurj.org

Stable Triarylmethyl Radicals and Cobalt(II) Ions Based 1D/2D Coordination Polymers

Xudong Hou[+],[a] Giang Truong Nguyen[+],[a] Tingting Xu,[a] Haipeng Wei,[a] Tun Seng Herng,[b] Guifei Huo,[a] Dingguan Wang,[a] Jun Ding,[b] Shaofei Wu,*[a] Liviu Ungur,*[a] and Jishan Wu*[a]

Abstract: The incorporation of organic radicals into coordination polymers was considered as a promising strategy to promote metal-ligand exchange interactions, but there are only a very limited number of stable organic radical-based ligands that can serve well such a purpose. Herein, we report two new tris(2,4,6-trichlorophenyl)methyl (TTM) radical-based ligands **L1** and **L2** with two and three imidazole substituents, respectively. The imidazole unit serves as a coordination site and it can also stabilize the TTM radical by intramolecular donor–acceptor interaction. Coordination of **L1** and **L2** with cobalt(II) ions gave the corresponding one- (**CoCP-1**) and two-dimensional (**CoCP-2**) coordination polymers, the structures of which were confirmed by X-ray crystallographic analysis. Magnetic measurements and theoretical calculations suggest antiferromagnetic coupling between the paramagnetic cobalt(II) ions and the radical ligands. Our study provides a rational design for stable organic radical-based ligands and further demonstrated the feasibility of a metal–radical approach toward magnetic materials.

Magnetically active metal–organic frameworks (MOFs) or coordination polymers (CPs) have promising applications for spintronics, molecular magnets and quantum information processing.[1] Traditionally, paramagnetic transition-metal or lanthanide ions are coordinated with nonmagnetic closed-shell ligands, and the magnetic exchange coupling between the nearby metal ions usually occurs through a relatively weak super-exchange mechanism.[2] Therefore, it remains a significant challenge to achieve strong magnetic coupling and long-range magnetic order. One possible solution to this end is the incorporation of open-shell organic radical ligands, the so-called radical–metal approach.[3] The efficient overlap of the magnetic orbitals of the metal ions and the paramagnetic radical ligand would significantly promote the exchange interactions. This concept has been validated by a number of open-shell CPs with nitroxide,[4] organonitrile,[5] semiquinoid,[6] and pyrazine[7] based radicals as ligands. Among them, nitroxide radicals are most stable but they have relatively localized spin distribution, and the other radicals are normally generated by in situ redox reactions and are sensitive to air and moisture. Therefore, stable organic radicals with delocalized spin distribution are ideal ligands, which not only maintain significant magnetic exchange interaction but also provide sufficient stability for coordination chemistry.

Polychlorinated triphenylmethyl (**PTM**) radical (Scheme 1a) has demonstrated very good thermal and chemical stability,[8] and thus was chosen as the fundamental building block to design stable radical-based ligands with one or more coordination groups.[9] For example, Veciana and co-workers reported a

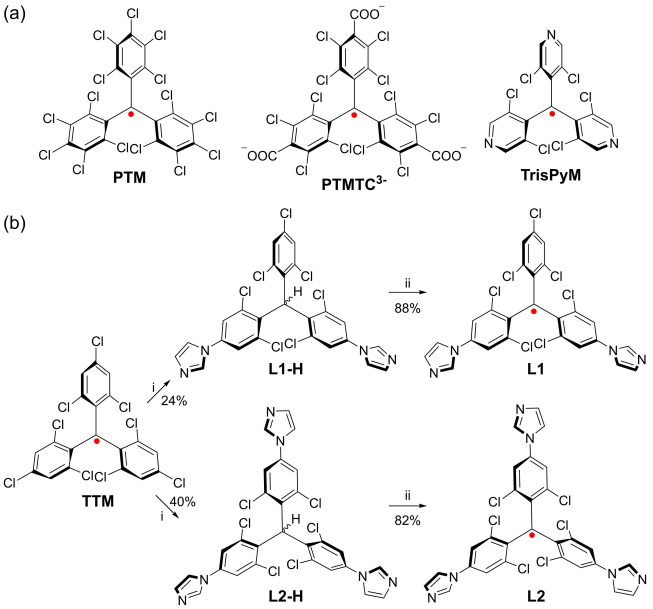

Scheme 1. (a) Structures of **PTM** and related ligands for metal–organic radical complexes and frameworks; (b) Synthesis of new imidazole-substituted TTM ligands **L1** and **L2**: (i) imidazole (6.4 equiv.), anhydrous Cs_2CO_3, DMF, 160 °C; (ii) $nBu_4N{\cdot}OH$ and then *p*-chloranil, THF, RT.

[a] *X. Hou,[+] G. Truong Nguyen,[+] T. Xu, Dr. H. Wei, Dr. G. Huo, Dr. D. Wang, Dr. S. Wu, Prof. L. Ungur, Prof. J. Wu*
Department of Chemistry
National University of Singapore
3 Science drive 3, 117543 Singapore (Singapore)
E-mail: chmswu@nus.edu.sg
chmlu@nus.edu.sg
chmwuj@nus.edu.sg

[b] *Dr. T. Seng Herng, Prof. J. Ding*
Department of Materials Science and Engineering
National University of Singapore
119260 Singapore (Singapore)

[+] *These authors contributed equally to this work.*

Supporting information for this article is available on the WWW under https://doi.org/10.1002/chem.202200687

trigonal, carboxylate-terminated PTM radical ligand (**PTMTC**$^{3-}$), which can coordinate with a Cu(II) ion to form a crystalline open-shell CP.[9c] The obtained framework showed a reversible and highly selective solvent-induced shrinking-breathing process which strongly influenced the material's magnetic properties. Alternatively, Nishihara and coworkers developed a pyridine-substituted triarylmethyl radical, which demonstrated ferromagnetic coupling with the Cu(II) ion.[10] Very recently, the same team reported a new trigonal ligand, the tris(3,5-dichloro-4-pyridyl)methyl radical (**trisPyM**, Scheme 1a), which formed hexagonal honeycomb lattice when coordinated with Zn(II) ions.[11] The obtained CPs exhibited intriguing solid-state luminescence and magnetoluminescence phenomenon. However, CPs using this ligand and paramagnetic transition-metal ions are not reported. In this study, two imidazole-substituted tris(2,4,6-trichlorophenyl)methyl (**TTM**) radicals, 2,6-dichloro-4-bis(2,6-dichloro-4-(1H-imidazol-1-yl)phenyl)(2,4,6-trichlorophenyl)methyl (**L1**) and tris(2,6-dichloro-4-(1H-imidazol-1-yl)phenyl)methyl radical (**L2**), were designed and synthesized as new radical ligands (Scheme 1b). The imidazole unit was chosen because its pyridinic-type nitrogen atom can serve as a coordination site while the other pyrrolic-type nitrogen atom can behave as an electron-donating site to enhance intramolecular donor–acceptor interaction (i.e., the TTM moiety as an electron acceptor). Such a captodative effect is expected to improve the stability of the organic radicals.[12] Coordination of these two ligands with paramagnetic Co(II) ions gave the corresponding one-dimensional (1D) CP **CoCP-1** and two-dimensional (2D) CP **CoCP-2** in single-crystal form. Antiferromagnetic coupling between the radical ligands and the Co(II) ions in both polymers was suggested by magnetic measurements and theoretical calculations.

The synthesis of these two ligands started with nucleophilic substitution reaction of the **TTM** radical[13] by excessive imidazole (6.4 equiv) in the presence of Cs_2CO_3 in DMF at 160 °C, giving the di- and tri-substituted intermediates **L1-H** and **L2-H** in 24% and 40% yield, respectively (Scheme 1b). That means simultaneous hydrogen abstraction happened during the reaction. Subsequent deprotonation by base (nBu$_4$N·OH) in THF followed by oxidation with *p*-chloranil afforded the target ligands **L1** and **L2** as stable materials that can be purified by routine column chromatography.

Compounds **TTM**, **L1** and **L2** in dichloromethane (DCM) show an intense absorption band with maximum (λ_{max}) at 373, 380 and 392 nm, respectively (Figure 1a and Figure S1 in the Supporting Information). According to the time-dependent density functional theory (TD DFT) calculations, this band is mainly correlated to the SOMO(α)→LUMO(α) and SOMO(α)→LUMO + 1(α) electronic transitions (see Supporting Information). With the introduction of two and three imidazole units, the energies of the SOMO(α) slightly increase while that of the LUMO(α) decrease (Figures S9–S11 in Supporting Information), leading to a convergence of the energy gap, in agreement with the experimental observation. In addition, weak bands with the lowest-energy absorption maximum at 542 (**TTM**), 554 (**L1**) and 560 nm (**L2**) are also observed, which can be mainly correlated to HOMO(β)→LUMO(β) and HOMO-1(β)→LUMO(β) electronic transitions. Compounds **TTM**, **L1** and **L2** also exhibit doublet emission[14] with corresponding photoluminescence quantum yield and emission maximum (λ_{em}) to be 0.8% (568 nm), 12% (588 nm), and 10.5% (591 nm), respectively (Figure 1a). Air-saturated solutions of **TTM**, **L1** and **L2** in DCM (1×10^{-4} M) under dark conditions are very stable, without obvious change of the absorption spectra after one week (Figure S2 in Supporting

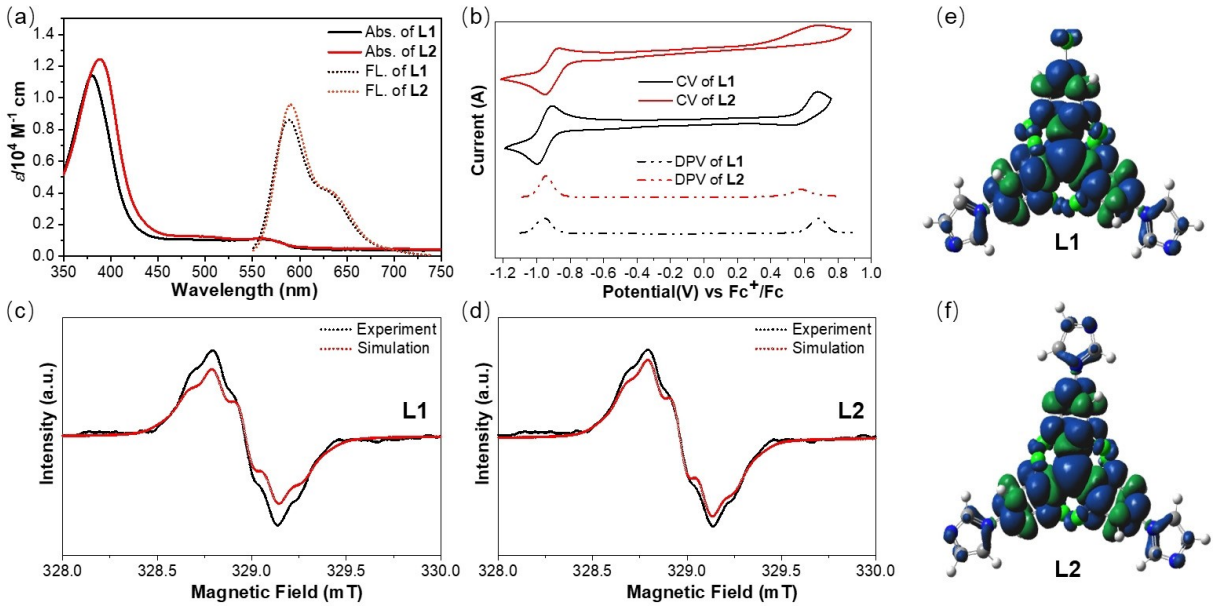

Figure 1. (a) UV-vis absorption (Abs) and normalized fluorescence (FL) spectra of **L1** and **L2** in DCM. The excitation wavelengths for FL are 382 and 393 nm, respectively; (b) Cyclic voltammograms and differential pulse voltammograms of **L1** and **L2** in DCM (with 0.1 M nBu$_4$NPF$_6$ as supporting electrolyte, scan rate: 100 mV/s for CV). (c) and (d): ESR spectra of **L1** and **L2** recorded in DCM at RT together with the simulated spectra. (e) and (f): calculated (UB3LYP/6-31G(d,p))spin density distribution maps for the **L1** and **L2** (isovalue: 0.0004).

Information). However, the solutions underwent degradation upon exposure to the ambient light, with a half-lifetime of about 723, 922 and 983 s for **TTM**, **L1** and **L2**, respectively (Figure S3 in Supporting Information). The improved photostability after the introduction of imidazole group could be explained by the intramolecular donor–acceptor interaction in the excited state, or captodative effect,[12] as previously demonstrated in other carbazole or triphenylamine-substituted PTM radicals.[15]

Cyclic voltammetry (CV) and differential pulse voltammetry (DPV) measurements of **TTM**, **L1** and **L2** in DCM all revealed one reversible oxidation wave and one reversible reduction wave (Figure 1b and Figure S4 in Supporting Information). The half-wave potential for the oxidation/reduction wave was determined to be 0.76/-0.97, 0.67/-0.96 V and 0.58/−0.95 V (vs. Fc^+/Fc) for **TTM**, **L1** and **L2**, respectively. Therefore, increasing the number of imidazole groups in **TTM** leads to the rising of the SOMO and lowering of the LUMO energy level, and consequently, a convergence of the electrochemical energy gap (Figure S12 in Supporting Information). At room temperature (RT), **TTM**, **L1** and **L2** in DCM showed a well-resolved ESR spectrum, with a *g* value of 2.0034, 2.0034 and 2.0036, respectively, all are correlated to carbon-centered radicals (Figure 1c, 1d and Figure S5 in Supporting Information). The observed ESR spectra agree with the simulation when considering the hyperfine coupling between the spin with the protons on the aryl substituents (Figure S6 in Supporting Information). The calculated spin density distribution maps suggest that the spin can be distributed from the center to the peripheries, with the highest spin density at the methylene sites (ca. 0.752) and small spin density at the terminal imine nitrogen atom (ca. 0.004) on the imidazole (Figure 1e, 1 f).

Under the dark condition, a solution of $CoCl_2$ in ethanol was layered onto the solution of **L1** in DMF and slow diffusion over 1–2 weeks yielded dark red crystals. X-ray crystallographic analysis of the crystal revealed the formation of a 1D CP named as **CoCP-1** ($CoCl_2(L1)_2$•$(DMF)_2$).[16] The molecules crystallized in a triclinic space group *P*1. In the asymmetric unit, the Co ion is coordinated by four N atoms of four **L1** radical ligands and two chlorine atoms of $CoCl_2$, resulting in a distorted CoN_4Cl_2-type octahedral coordination polyhedron with adjacent angles in the range of 87.40–92.60° (Figure 2a). The equatorial position of the octahedron is occupied by four bridging **L1** radical ligands, forming chains along [0 0 1] direction. The Co–N bond lengths fall in the range between 2.123(4) Å and 2.157(4) Å. The interchain [Cl···Cl] close contacts are observed, which stabilize the crystal structure along [101] direction (Figure 2b). Schematic illustration of the coordination environment and the positions of the spins of one layer are depicted in Figure 2e for **CoCP-1**. The spin centers of **CoCP-1** are located at the vertices of a parallelogram lattice with C_{center}–Co_{center} distances of 9.762 and 9.806 Å. Under similar reaction conditions, slow diffusion between the solution of cobalt(II) triflimide ($Co(NTf)_2$) in ethanol and **L2** in DMF yielded hexagonal-shaped dark red single crystals. X-ray crystallographic analysis disclosed formation of a 2D CP named as **CoCP-2** ($Co(NTf)_2(L2)_2 \cdot (DMF)_2$), which crystallized in R-3 space group.[16] The asymmetric unit is composed of one Co(II) ion with 1/6 occupancy, and one ligand with 1/3 occupancy. The metal center is coordinated with six nitrogen atoms of six independent **L2** radical ligands, resulting in a distorted CoN6-type octahedral coordination polyhedron with an adjacent angle of 90.0(2)° (Figure 2d), and the dihedral angles between phenylene and imidazole become smaller (ca. 6.8°) after coordination with cobalt(II) ions. The analysis also

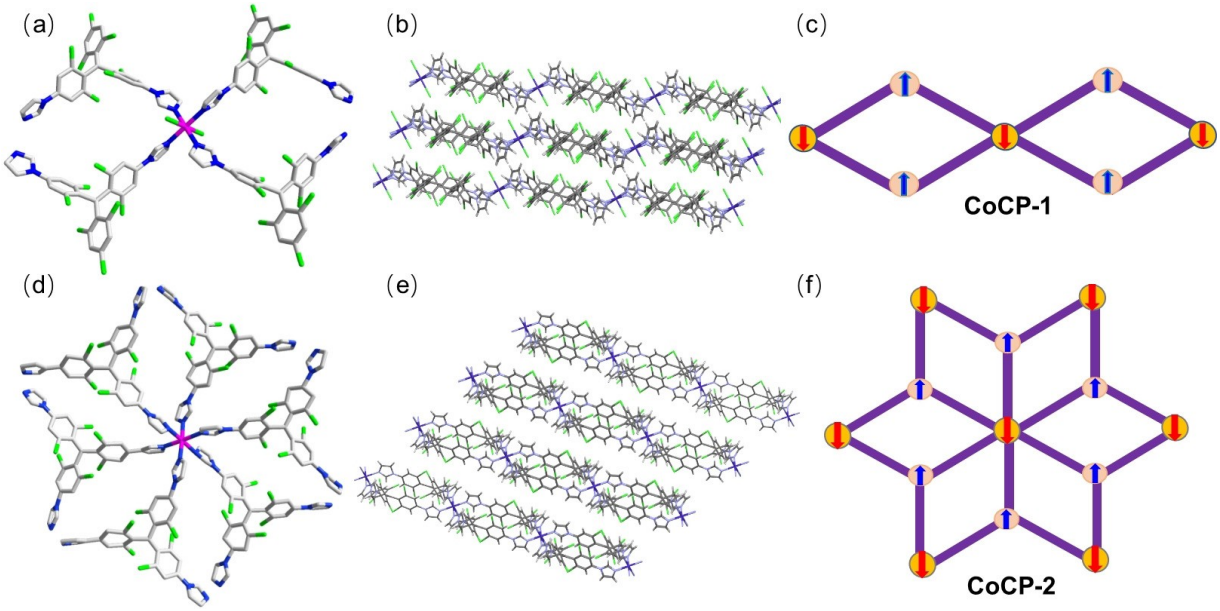

Figure 2. Crystallographic graph for **CoCP-1** (a) and **CoCP-2** (d), 3D packing layer-like structures of **CoCP-1** (b) and **CoCP-2** (e), and schematic illustration of the coordination environment and the arrangement of the spins in one layer of **CoCP-1** (c) and **CoCP-2** (f). Hydrogen atoms, solvents and disordered anions have been omitted for clarity.

reveals that **CoCP-2** has a $(4^6 6^6 8^3)(4^3)_2$-connected binodal *kgd* topology, which is not commonly found in metal–organic frameworks.[17] The 2D CPs are then packed into a layer-like structure via Van der Waals interaction (Figure 2e). The coordination environment and the spin positions of **CoCP-2** are shown in Figure 2f. The spin centers of **CoCP-2** are located at the vertices of a pseudo-hexagon lattice with C_{center}—Co_{center} distances of 9.695 Å and 9.763 Å. The phase purity and crystallinity of **CoCP-1** and **CoCP-2** were further confirmed by powder X-ray diffraction (Figures S19 and S20 in Supporting Information).

Both **CoCP-1** and **CoCP-2** are characterized by broad absorption bands in the UV-vis region (Figure 3a). For **CoCP-1**, the band with λ_{max} at 385 nm could be correlated to the π-π* transition of the ligands, while the bands with λ_{max} at 470/508 and the shoulder at 720 nm are features of high-spin, octahedrally coordinated Co(II) complexes.[18] The band with λ_{max} at 553 nm could be attributed to the coexistence of the absorption from the carbon-centered radicals and heavy atom effect of Co(II). **CoCP-2** shows a similar absorption spectrum but with a distinct red-shift as compared to **CoCP-1**, which can be interpreted as a consequence of topological extension from 1D to 2D. Broad ESR signals with *g* value at around 2.003 were observed in both **CoCP-1** and **CoCP-2**, in accordance with the presence of the open-shell radical ligands (Figure 3b). In addition, an intense one-line ESR signal was also found with *g* value around 4.25, which can be correlated to the paramagnetic Co(II) ion (Figure S8 and Tables S7, S10 in Supporting Information).[19]

The temperature-dependent magnetic susceptibility of the as-prepared crystalline samples of **CoCP-1** and **CoCP-2** was measured by superconducting quantum interference device (SQUID). In both cases, the product of the molar magnetic susceptibility (χ_M in emu·mol^{-1}) and temperature (T in K) decreased upon cooling from 300 K down to 2 K (Figure 4). For **CoCP-1**, the measured $\chi_M T$ value of 3.2 emu·K·mol^{-1} at 300 K is much higher than the spin-only value of 2.625 emu·K·mol^{-1} expected for one uncoupled $S=3/2$ high-spin octahedral Co(II) center and two carbon radical units ($S=1/2$). Such deviation can be attributed to the orbital contribution of Co(II), which is known to be significant in an octahedral field.[20] Upon lowering the temperature, the $\chi_M T$ value decreased continuously down to 1.66 emu·K·mol^{-1} at 3.0 K. For **CoCP-2**, the $\chi_M T$ value is determined as 5.114 emu·K·mol^{-1} at 300 K, which is also higher than the expected for non-interacting Co(II) ions and carbon radicals, with a 1:2 stoichiometry and local spins $S(Co^{2+})=3/2$, S(**L2**)=1/2. The $\chi_M T$ decreased gradually to reach a minimum value of 1.55 emu·K·mol^{-1} at 4 K, which is similar to the value of **CoCP-1**. Quantitative analysis and fitting of the magnetic data are very challenging due to the complicated electron structure of the Co(II) ions and possibly partial oxidation of the high-spin Co(II) to low-spin Co(III) ions, which was further confirmed by band valence analysis and XPS measurements (Figures S21, S22, Tables S15, S16, S17 in Supporting Information).[21]

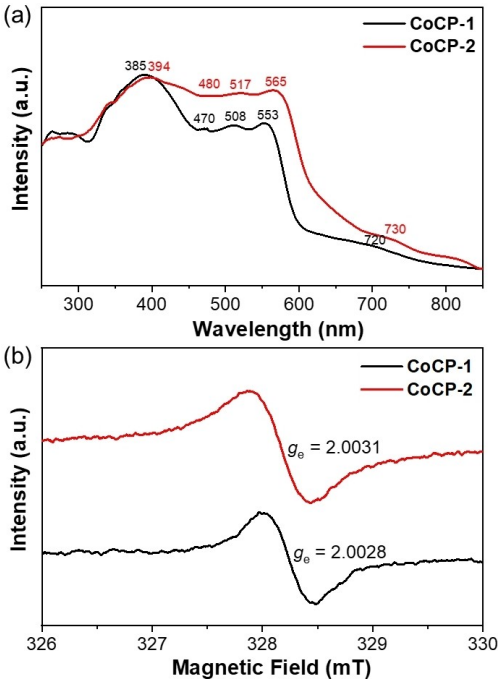

Figure 3. (a) Solid-state UV-visible absorption spectra of **CoCP-1** and **CoCP-2**; (b) partial ESR spectra of **CoCP-1** and **CoCP-2** in solid state at RT.

To understand the ground-state electronic properties and magnetic exchange interactions between the radicals and the Co(II) ions, ab initio quantum mechanical calculations were conducted based on the crystallographic structures (see details in Supporting Information). In both CPs, Co(II) ions are found to be in a high-spin quartet ($S=3/2$) ground state, which is about 10 kcal/mol lower than the doublet ($S=1/2$) excited state (Table S11 in Supporting Information). Multireference CASSCF-SO calculations show that the ground state is near-degenerate, originating from the octahedral $^4T_2$ term subject to weak splitting due to the departure from ideal O_h symmetry and second coordinated ligand atoms. In this case, spin-orbit coupling is effective at first order of perturbation theory and therefore mixes efficiently the low-lying spin quartet states of $^4T_2$ giving rise to six Kramers doublets (Tables S6 and S9). The joint effect of spin-orbit coupling and the departure from ideal O_h symmetry leads to on-site magnetic anisotropy, reflected in the *g*-tensors of the low-lying spin-orbit doublet states (Tables S7 and S10). In both compounds **CoCP-1** and **CoCP-2** the magnetic anisotropy of ground doublet state is of easy-plane type while the first excited doublet state displays easy-axis anisotropy. Broken symmetry

DFT calculations predicted antiferromagnetic coupling between the Co(II) ion and the radical ligands, with *J* value in the range of $-2\sim-5$ cm^{-1} (Tables S12, S13 in Supporting Information). The calculated spin density distribution map of the individual coordination unit shows spin delocalization across the metal ion and ligands (Figure 4c, 4d), presumably due to the non-orthogonal arrangement of the *d*-orbital of the Co(II) ion and the *p*-orbital of the imidazole moiety. On the other hand, the metal-metal and radical-radical exchange interactions are calculated to be ferromagnetic, with *J* value less than 1.3 cm^{-1}. The temperature-dependent magnetic susceptibility

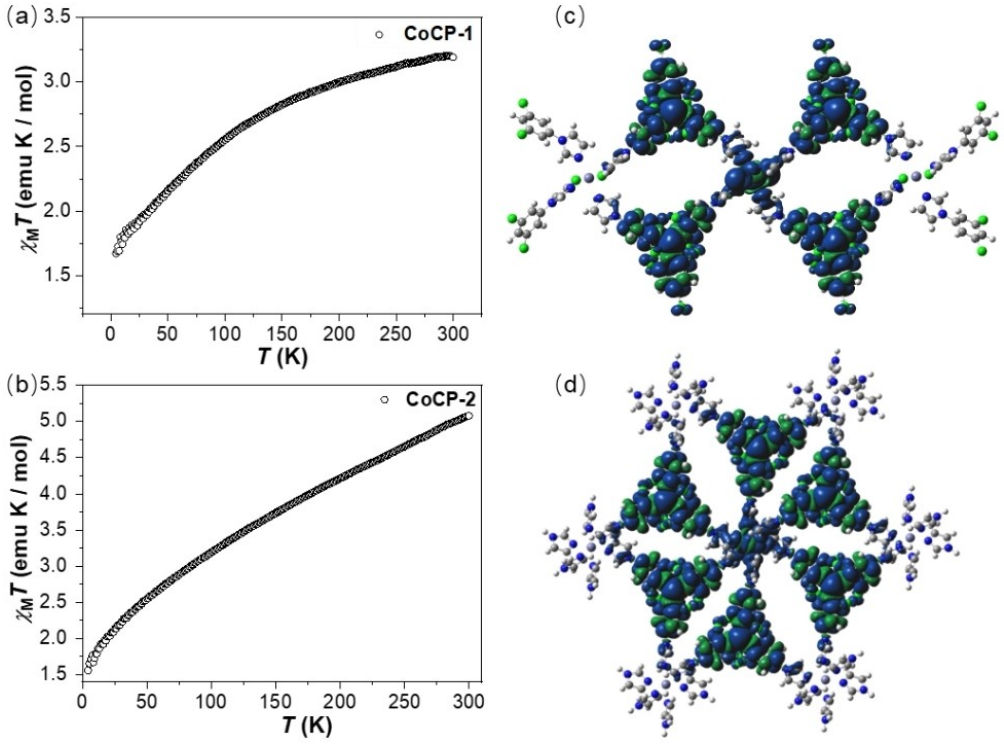

Figure 4. Temperature dependent molar magnetic susceptibility (χ_M) of **CoCP-1** (a) and **CoCP-2** (b), calculated spin density distribution maps for the subunits of **CoCP-1** (c) and **CoCP-2** (d) (isovalue: 0.0004).

thus can be mainly explained by the Co(II) ions with multiple spin-orbit coupling doublets, with a certain contribution from the antiferromagnetic coupling between the Co(II) ions and the radical ligands.

In summary, we developed two new imidazole-substituted TTM radical ligands by simple reactions. Both ligands are stable due to the intramolecular donor–acceptor interaction and captodative effect, which allowed us to construct 1D and 2D open-shell coordination polymers with high-spin Co(II) ions. Notably, both polymers show antiferromagnetic coupling between the Co(II) ions and the radical ligands, again supporting the feasibility of radical-metal approach. Further research on imidazole-based organic radical ligands and open-shell CPs with enhanced metal–radical exchange interaction is ongoing in our lab.

Acknowledgements

J. W. acknowledges financial support from NRF Investigatorship (NRF-NRFI05-2019-0005) and MOE Tier 2 project (MOE2019-T2-1-030). S. W. thanks the financial support from the A*STAR AME YIRG project (A2084c0164). X. Hou thanks the scholarship support from the China Scholarship Council (CSC). L.U. acknowledges the financial support of the research projects R-143-000-A65-133 and R-143-000-A80-114 of the National University of Singapore. Ab initio calculations were done on the ASPIRE-1 cluster (www.nscc.sg) under the project 11001278. G. T. N. was supported by the NUS Research Scholarship program.

Conflict of Interest

The authors declare no conflict of interest.

Data Availability Statement

The data that support the findings of this study are available from the corresponding author upon reasonable request.

Keywords: cobalt ion · magnetic property · open-shell coordination polymer · stable organic radical · triarylmethyl radical

[1] a) T. B. Faust, D. M. D'Alessandro, *RSC Adv.* **2014**, *4*, 17498–17512; b) A. E. Thorarinsdottir, T. D. Harris, *Chem. Rev.* **2020**, *120*, 8716–8789.
[2] M. Kurmoo, *Chem. Soc. Rev.* **2009**, *38*, 1353–1379.
[3] A. Caneschi, D. Gatteschi, R. Sessoli, P. Rey, *Acc. Chem. Res.* **1989**, *22*, 392–398.
[4] a) H. O. Stumpf, L. Ouahab, Y. Pei, D. Grandjean, O. Kahn, *Science* **1993**, *261*, 447–449; b) H. O. Stumpf, L. Ouahab, Y. Pei, P. Bergerat, O. Kahn, *J. Am. Chem. Soc.* **1994**, *116*, 3866–3874; c) K. Inoue, H. Iwamura, *J. Am. Chem. Soc.* **1994**, *116*, 3173–3174; d) K. Inoue, T. Hayamizu, H. Iwamura, D. Hashizume, Y. Ohashi, *J. Am. Chem. Soc.* **1996**, *118*, 1803–1804; e) K. Fegy, D. Luneau, T. Ohm, C. Paulsen, P. Rey, *Angew. Chem. Int. Ed.* **1998**, *37*, 1270–1273; *Angew. Chem.* **1998**, *110*, 1331–1335.

[5] a) J. M. Manriquez, G. T. Yee, R. S. McLean, A. J. Epstein, J. S. Miller, *Science* **1991**, *252*, 1415–1417; b) H. Miyasaka, T. Izawa, N. Takahashi, M. Yamashita, K. R. Dunbar, *J. Am. Chem. Soc.* **2006**, *128*, 11358–11359; c) K. I. Pokhodnya, M. Bonner, J.-H. Her, P. W. Stephens, J. S. Miller, *J. Am. Chem. Soc.* **2006**, *128*, 15592–15593; d) N. Motokawa, H. Miyasaka, M. Yamashita, K. R. Dunbar, *Angew. Chem. Int. Ed.* **2008**, *47*, 7760–7763; *Angew. Chem.* **2008**, *120*, 7874–7877; e) K. H. Stone, P. W. Stephens, A. C. McConnell, E. Shurdha, K. I. Pokhodnya, J. S. Miller, *Adv. Mater.* **2010**, *22*, 2514–2519.

[6] a) I.-R. Jeon, B. Negru, R. P. Van Duyne, T. D. Harris, *J. Am. Chem. Soc.* **2015**, *137*, 15699–15702; b) J. A. DeGayner, I.-R. Jeon, L. Sun, M. Dincă, T. D. Harris, *J. Am. Chem. Soc.* **2017**, *139*, 4175–4184; c) L. Liu, J. A. DeGayner, L. Sun, D. Z. Zee, T. D. Harris, *Chem. Sci.* **2019**, *10*, 4652–4661.

[7] K. S. Pedersen, P. Perlepe, M. L. Aubrey, D. N. Woodruff, S. E. Reyes-Lillo, A. Reinholdt, L. Voigt, Z. Li, K. Borup, M. Rouzières, D. Samohvalov, F. Wilhelm, A. Rogalev, J. B. Neaton, J. R. Long, R. Clérac, *Nat. Chem.* **2018**, *10*, 1056–1061.

[8] I. Ratera, J. Veciana, *Chem. Soc. Rev.* **2012**, *41*, 303–349.

[9] a) D. Maspoch, D. Ruiz-Molina, K. Wurst, C. Rovira, J. Veciana, *Chem. Commun.* **2002**, 2958–2959; b) D. Maspoch, N. Domingo, D. Ruiz-Molina, K. Wurst, J. M. Hernandez, G. Vaughan, C. Rovira, F. Lloret, J. Tejada, J. Veciana, *Chem. Commun.* **2005**, 5035–5037; c) D. Maspoch, D. Ruiz-Molina, K. Wurst, N. Domingo, M. Cavallini, F. Biscarini, J. Tejada, C. Rovira, J. Veciana, *Nat. Mater.* **2003**, *2*, 190–195.

[10] T. Kusamoto, Y. Hattori, A. Tanushi, H. Nishihara, *Inorg. Chem.* **2015**, *54*, 4186–4188.

[11] a) S. Kimura, M. Uejima, W. Ota, T. Sato, S. Kusaka, R. Matsuda, H. Nishihara, T. Kusamoto, *J. Am. Chem. Soc.* **2021**, *143*, 4329–4338; b) S. Kimura, R. Matsuoka, S. Kimura, H. Nishihara, T. Kusamoto, *J. Am. Chem. Soc.* **2021**, *143*, 5610–5615.

[12] a) H. G. Viehe, Z. Janousek, R. Merényi, L. Stella, *Acc. Chem. Res.* **1985**, *18*, 148–154; b) T. R. Albright, A. H. Winter, *J. Am. Chem. Soc.* **2015**, *137*, 3402–3410.

[13] O. Armet, J. Veciana, C. Rovira, J. Riera, J. Castaner, E. Molins, J. Rius, C. Miravitlles, S. Olivella, J. Brichfeus, *J. Phys. Chem.* **1987**, *91*, 5608–5616.

[14] a) Y. Hattori, T. Kusamoto, H. Nishihara, *Angew. Chem. Int. Ed.* **2014**, *53*, 11845–11848; *Angew. Chem.* **2014**, *126*, 12039–12042; b) Q. Peng, A. Obolda, M. Zhang, F. Li, *Angew. Chem. Int. Ed.* **2015**, *54*, 7091–7095; *Angew. Chem.* **2015**, *127*, 7197–7201.

[15] a) H. Guo, Q. Peng, X.-K. Chen, Q. Gu, S. Dong, E. W. Evans, A. J. Gillett, X. Ai, M. Zhang, D. Credgington, V. Coropceanu, R. H. Friend, J.-L. Brédas, Feng Li, *Nat. Mater.* **2019**, *18*, 977–984; b) E. Cho, V. Coropceanu, J.-L. Brédas, *J. Am. Chem. Soc.* **2020**, *142*, 17782–17786.

[16] Deposition Numbers 2121338 (**CoCP-1**) and 2128896 (**CoCP-2**) contains the supplementary crystallographic data for this paper. These data are provided free of charge by the joint Cambridge Crystallographic Data Centre and Fachinformationszentrum Karlsruhe Access Structures service.

[17] a) A. V. Desai, A. Roy, P. Samanta, B. Manna, S. K. Ghosh, *iScience* **2018**, *3*, 21–30; b) S. R. Zheng, Q. Y. Yang, Y. R. Liu, J. Y. Zhang, Y. X. Tong, C. Y. Zhao, C. Y. Su, *Chem. Commun.* **2008**, 356–358.

[18] a) M.-H. Zeng, B. Wang, X.-Y. Wang, W.-X. Zhang, X.-M. Chen, S. Gao, *Inorg. Chem.* **2006**, *45*, 7069–7076; b) Y. W. Li, S. J. Liu, T. L. Hu, X. H. Bu, *Dalton Trans.* **2014**, *43*, 11470–11473.

[19] M. E. Foglioa, M. C. dos Santosa, G. E. Barberisa, J. M. Rojob, J. L. Mesab, L. Lezamab, T. Rojo, *Physica B + C* **2002**, *320*, 423–426.

[20] a) M.-H. Zeng, M.-X. Yao, H. Liang, W.-X. Zhang, X.-M. Chen, *Angew. Chem. Int. Ed.* **2007**, *46*, 1832–1835; *Angew. Chem.* **2007**, *119*, 1864–1867; b) D. Maspoch, N. Domingo, D. Ruiz-Molina, K. Wurst, J. M. Hernandez, G. Vaughan, C. Rovira, F. Lloret, J. Tejada, J. Veciana, *Chem. Commun.* **2005**, 5035–5037.

[21] Y. W. Li, S. J. Liu, T. L. Hu, X. H. Bu, *Dalton Trans.* **2014**, *43*, 11470–11473.

Manuscript received: March 3, 2022
Accepted manuscript online: March 23, 2022
Version of record online: April 13, 2022